Comparison of the ENATE approach and discontinuous Galerkin spectral element method in 1D nonlinear transport equations*

Víctor Llorente[1], Gonzalo Rubio[3], Antonio Pascau[1]
Esteban Ferrer[3], Müslüm Arıcı[1,2]
[1] *Fluid Mechanics Group and LIFTEC, University of Zaragoza and CSIC*
Zaragoza 50018, Spain
e-mail: pascau@unizar.es
[2] *Mechanical Engineering Department, Umuttepe Campus, Kocaeli University*
Kocaeli 41380, Turkey
[3] *Applied Mathematics and Statistics Department, Polytechnical University of Madrid*
Madrid 28040, Spain

In this paper a comparison of the performance of two ways of discretizing the nonlinear convection-diffusion equation in a one-dimensional (1D) domain is performed. The two approaches can be considered within the class of high-order methods. The first one is the discontinuous Galerkin method, which has benn profusely used to solve general transport equations, either coupled as the Navier-Stokes equations, or on their own. On the other hand, the ENATE procedure (Enhanced Numerical Approximation of a Transport Equation), uses the exact solution to obtain an exact algebraic equation with integral coefficients that link nodal values with a three-point stencil. This paper is the first of a thorough assessment of ENATE by comparing it with well established high-order methods. Several test cases of the steady Burgers' equation with and without source have been chosen for comparison.

Keywords: one-dimensional transport equation, high-order methods.

1. Introduction

There are several physical phenomena governed by transport equations. In fluid mechanics these equations represent the evolution at length and time-scales of interest (fluid particle) of phenomena usually occurring at a much smaller scale (molecule). The values that a certain variable attains in the domain are those that satisfy a balance between several fluxes written mathematically in terms of (normally) first and second derivatives. The convection-diffusion equation that governs the transport of a scalar field is one of these equations.

There are hardly any analytical solutions to transport equations, which would be of interest, so in order to provide answers to engineering or physical problems one has to resort to numerical approximations. There is a wealth of numerical approaches to the discretization of transport equations: finite volumes, finite elements or spectral elements, among others. Although the first discretization schemes used were only first order there has been a huge increase along the years in the order of the schemes routinely employed, as well as a considerable improvement in their robustness. In this paper two high-order methods will be compared, one is the well established discontinuous Galerkin spectral element method (DGSEM) [23], which belongs to the family of discontinuous Galerkin methods and the other is recently proposed ENATE. ENATE is a finite volume

* The paper was presented during the Eurotherm Seminar No 109 – Numerical Heat Transfer 2015.

approach that has been introduced in two recent papers [26, 27]. The latter technique provides the exact solution for a 1D convection-diffusion equation with arbitrary coefficients and source, if some integrals related to the scheme are exact. Its derivation uses the exact solution of a second-order ordinary differential equation (ODE) to build an exact algebraic connection between nodal values. On the other hand, the DGSEM shares some ideas with the finite element method and the spectral discretization communities. A brief description of both will be given in this paper.

The paper is structured as follows. A brief description of the two approaches employed is given in the first section. In the results section both are compared in several cases related to the 1D steady Burgers' equation, with and without source term. The source is chosen so as to provide a smooth sinusoidal solution. Although the solution is very smooth the source is not simple due to the equation nonlinearity, so the ability of the approaches to deal with non-trivial sources can be checked. Finally, some conclusions are drawn and several avenues of further research are suggested.

2. Description of the approaches

2.1. ENATE

The 1D convection-diffusion equation with variable coefficients can be written as

$$\frac{d}{dx}\left(\rho v\phi - \Gamma\frac{d\phi}{dx}\right) = S, \tag{1}$$

where v is the advective velocity, ρ is the density, Γ is the diffusion coefficient, ϕ denotes the unknown variable, and S is a source term. In ENATE the domain is split in K intervals, not necessarily of equal length, and $K+1$ nodes with locations x_i, $i = 0, ..., K$, with two nodes at the boundaries, x_0 and x_K. The whole procedure utilizes normalized variables, defined in each interval as

$$\widehat{\phi} = \frac{\phi - \phi_{lb}}{\phi_{rb} - \phi_{lb}} = \frac{\phi - \phi_{lb}}{\Delta\phi}, \qquad \widehat{\rho v} = \frac{\rho v}{(\rho v)_{lb}}, \qquad \widehat{\Gamma} = \frac{\Gamma}{\Gamma_{lb}}, \qquad \widehat{\lambda} = \frac{\widehat{\rho v}}{\widehat{\Gamma}}. \tag{2}$$

In every interval, rb and lb stand for right and left boundaries respectively. All variables are normalized with their value at the left boundary of the interval and $\widehat{\lambda}$ is connected to the variation of the convective and diffusive fluxes over the reference interval. A normalized coordinate $\widehat{x}$ is also used in a generic interval of length $L = x_{rb} - x_{lb}$, defined by $x = x_{lb} + L\widehat{x}$, $0 \leqslant \widehat{x} \leqslant 1$, $x \in [x_{lb}, x_{rb}]$. By splitting the solution into the normalized homogeneous, $\overline{\phi}^N(\widehat{x})$, and particular solutions, $F(\widehat{x})$, the complete solution to the normalized transport equation can be shown to be

$$\widehat{\phi} = F(\widehat{x}) + (1 - F(1))\,\overline{\phi}^N(\widehat{x}). \tag{3}$$

The algebraic equation is obtained by explicitly deriving exact expressions for $F(\widehat{x})$ and $\overline{\phi}^N(\widehat{x})$ and applying continuity of diffusive fluxes at the interval edges. All algebraic details are in the abovementioned papers. For the case of a convection-diffusion equation with source the final expression is

$$\left[(\rho v)_W\,\widetilde{k}_{WP} + (\rho v)_P\left(\widetilde{k}_{PE} + \left.\frac{ILE_{01}}{IGE_{01}}\right|_{PE}\right)\right]\phi_P = (\rho v)_W\left(\widetilde{k}_{WP} + \left.\frac{ILE_{01}}{IGE_{01}}\right|_{WP}\right)\phi_W + (\rho v)_P\,\widetilde{k}_{PE}\phi_E + IS_{01}|_{WP} + \left(\left.\frac{ISGE_{01}}{IGE_{01}}\right|_{PE} - \left.\frac{ISGE_{01}}{IGE_{01}}\right|_{WP}\right). \tag{4}$$

The different factors that appear in the formulation are

$$ILE_{01} = \int_0^1 \frac{\widehat{\lambda}}{\overline{E}} d\widehat{x}', \qquad IGE_{01} = \int_0^1 \frac{d\widehat{x}'}{\widehat{\Gamma}\,\overline{E}}, \qquad \widetilde{k} = \frac{1}{P_{L0} IGE_{01}},$$

$$ISGE_{01} = \int_0^1 \frac{IS_{0\widehat{x}'}}{\widehat{\Gamma}\,\overline{E}} d\widehat{x}' = \int_0^1 \frac{L \int_0^{\widehat{x}'} S(\widehat{x}'') d\widehat{x}''}{\widehat{\Gamma}\,\overline{E}} d\widehat{x}', \tag{5}$$

$$IS_{01} = L \int_0^1 S(\widehat{x}) d\widehat{x} = \int_{x_{lb}}^{x_{rb}} S(x) dx, \qquad \overline{E}(\widehat{x}) = \exp\left(- \int_{\widehat{x}}^1 P_L d\widehat{x}' \right).$$

The Péclet numbers are defined as

$$P_{L0} = \frac{(\rho \upsilon)_{lb} L}{\Gamma_{lb}}, \qquad P_L = \frac{\rho \upsilon L}{\Gamma}. \tag{6}$$

In terms of these Péclet numbers $\widehat{\lambda}$ may be written as P_L/P_{L0}. Equation (4) provides an exact relationship between the nodal values. If the integrals were amenable to be calculated analytically then the exact nodal values would be obtained. Note that if the velocity is the unknown of the nonlinear equation both $\widehat{\lambda}$ and $\overline{E}(\widehat{x})$ are updated at every iteration based on the newly obtained values of υ. In this latter case the nondimensional diffusion coefficient $\widehat{\Gamma}$ is the nondimensional viscosity $\widehat{\mu}$ and all Péclet numbers in the previous equation are actually Reynolds numbers.

To calculate all integrals in the previous expression Hermite splines are employed as interpolants of the integrands. Cubic, quintic and septic Hermite polynomials are used. They require the values of the function to be interpolated at the edges of the interval and a number of derivatives that depend on the polynomial degree. In the formulation presented in this paper these can be estimated from the nodal values. The derivation and the whole expression that links nodal values and derivatives is given in [27]. For the sake of completeness the values of the derivatives of the velocity $\widehat{\upsilon}$ are given here for a general case with variable viscosity and source as

$$\frac{d\widehat{\upsilon}}{d\widehat{x}} = \mathrm{Re}_L \frac{\upsilon}{\Delta \upsilon} + \frac{1}{\widehat{\mu}} \frac{1 + \mathrm{Re}_{L0} (\widetilde{ISGE}_{01} - \frac{\upsilon_{lb}}{\Delta \upsilon} ILE_{01})}{IGE_{01}} - \frac{\mathrm{Re}_{L0}}{\widehat{\mu}} \int_0^{\widehat{x}} \Pi_s d\widehat{x}',$$

$$\Delta \upsilon = \upsilon_{rb} - \upsilon_{lb}, \tag{7}$$

$$\widetilde{ISGE}_{01} = \int_0^1 \frac{\int_0^{\widehat{x}} \Pi_s d\widehat{x}'}{\widehat{\Gamma}\,\overline{E}} d\widehat{x} = \frac{ISGE_{01}}{(\rho \upsilon)_{lb} \Delta \upsilon}.$$

The general expression is a bit cumbersome to handle but in the case of constant viscosity, $\widehat{\mu} = 1$, and no source, the derivatives are much simpler

$$\frac{d\widehat{\upsilon}}{d\widehat{x}} = \mathrm{Re}_L \frac{\upsilon}{\Delta \upsilon} + \frac{1 - \mathrm{Re}_{L0} \frac{\upsilon_{lb}}{\Delta \upsilon} ILE_{01}}{IGE_{01}} = \mathrm{Re}_L \frac{\upsilon}{\Delta \upsilon} + C_1,$$

$$\frac{d^2\widehat{\upsilon}}{d\widehat{x}^2} = \frac{1}{\Delta \upsilon} \frac{d}{d\widehat{x}} (\mathrm{Re}_L \upsilon) = \frac{1}{\mathrm{Re}_L^{(\Delta \upsilon)}} \frac{d}{d\widehat{x}} \mathrm{Re}_L^2, \tag{8}$$

$$\mathrm{Re}_L^{(\Delta \upsilon)} = \frac{\rho \Delta \upsilon L}{\mu}.$$

Let us note that C_1 is a constant, so it does not appear in high-order velocity derivatives what makes the n-th-order derivative very easy to calculate.

In the case of high Reynolds numbers the exponential of $\overline{E}$ can be very large at one end of the interval, varying very rapidly across it. As a result the quality of the approximating Hermite polynomials is reduced. This can produce negative values of integrals that should otherwise be positive. In this paper a transformation of the original exponential is employed

$$\frac{1}{\overline{E}} = \exp \int_{\widehat{x}}^{1} \mathrm{Re}_L d\widehat{x}' = \exp \int_{\widehat{x}}^{1} (\mathrm{Re}_L - \overline{\mathrm{Re}}_L) d\widehat{x}' \cdot \exp \int_{\widehat{x}}^{1} \overline{\mathrm{Re}}_L d\widehat{x}' = \exp \overline{\mathrm{Re}}_L (1-\widehat{x}) \cdot \exp \int_{\widehat{x}}^{1} (\mathrm{Re}_L - \overline{\mathrm{Re}}_L) d\widehat{x}'$$

$$= \exp \overline{\mathrm{Re}}_L (1-\widehat{x}) \cdot \exp \int_{0}^{1} (\mathrm{Re}_L - \overline{\mathrm{Re}}_L) d\widehat{x}' \cdot \exp \left(- \int_{0}^{\widehat{x}} (\mathrm{Re}_L - \overline{\mathrm{Re}}_L) d\widehat{x}' \right). \quad (9)$$

If we choose $\overline{\mathrm{Re}}_L = \int_0^1 \mathrm{Re}_L d\widehat{x}$ the second exponential is one and then

$$\frac{1}{\overline{E}} = \exp \overline{\mathrm{Re}}_L (1-\widehat{x}) \cdot \exp \left(- \int_{0}^{\widehat{x}} (\mathrm{Re}_L - \overline{\mathrm{Re}}_L) d\widehat{x}' \right). \quad (10)$$

The second exponential of the expression above is much more suitable for being approximated with Hermite splines.

The derivatives of the Péclet number can also be obtained from the velocity derivatives. They are employed when needed in the derivatives of the different integrands at the edges of the reference interval.

2.2. DGSEM

In the last decade, the discontinuous Galerkin (DG) method started to be widely used in the computational physics community. DG methods were first introduced by Reed and Hill [30] to solve the neutron transport equation. They have emerged in recent years as an efficient and flexible method to solve elliptic and convection-diffusion problems [4, 5]. Since, DG methods have proven useful in solving the compressible, e.g., [4], and the incompressible Navier-Stokes equations, e.g., [3, 15, 16].

The DGSEM [6, 22, 23] can be seen as a spectral element method (SEM) [8] where the continuity requirement across element boundaries is relaxed, or as a high-order FV method with a compact stencil. As in a usual FV method, the Riemann solver [34] stabilizes the solution. However, in this case, higher accuracy may be achieved by increasing the order of the approximation, N, as well as by reducing the size of the elements h. The advantage of high-order methods is that an exponential decrease of the error is obtained for increasing polynomial orders [14, 19]. For smooth solutions, the error reduces as h^P, where $h = \delta x$ is the mesh size and P is the polynomial order. The DGSEM is used in a wide range of applications such as compressible flows [7, 20, 21, 28], electromagnetics and optics [1, 10, 11, 24], heat transfer [25], aeroacoustics [9, 29, 32, 33], meteorology [17, 18, 31], and geophysics [12, 13].

The DGSEM [6] can be classified as a discontinuous nodal Galerkin method [23]. Regarding the bases used to approximate the function, Legendre polynomials are usually chosen, due to their unity weight function ($w(x) = 1$), which makes the integrals that arise in the weak form easier to evaluate. The integrals are approximated by quadrature and the Legendre Gauss (LG) nodes are chosen because of their higher accuracy, leading to the Lagrange representation. From a geometrical point of view, this is the multidomain method, which means that the physical domain is divided

into subdomains where the solution is approximated. The method is called "discontinuous" since no continuity requirements are enforced at the interface of the elements.

The DG methods were originally developed to solve conservation laws [30]. Here we detail the 1D formulation that can be extended to multiple dimensions,

$$\phi_t + f_x = S, \qquad x \in (0, L), \tag{11}$$

where f is the flux function, f_x denotes its spatial derivative, ϕ is the unknown variable and S is a source term. For the sake of simplicity, the source term will be considered equal to zero, $S = 0$, in the derivation. Notice that, in general, $f(\phi) = f_A(\phi) - f_V(\phi)$ where $f_A(\phi)$ is the advective flux and $f_V(\phi)$ is the viscous flux. Taking $f_A(\phi) = \rho\upsilon\phi$ and $f_V(\phi) = \Gamma\phi_x$, Eq. (1) is recovered.

To motivate the derivation of the DGSEM the conservation law is discretized, the steady convection-diffusion equation is then obtained by dropping the time derivative term. As the method is of Galerkin type, the conservation law is written in variational form,

$$\int_{x_k-1}^{x_k} (\phi_t + f_x)\,\psi dx = 0, \qquad x \in (0, L), \tag{12}$$

where ψ is a local smooth test function. The interval $[0, L]$ is divided into K subdomains $\Omega^k = [x_{k-1}, x_k]$, (as can be seen in Fig. 1) and the integral splits into the sum of element integrals,

$$\sum_{k=1}^{K} \left\{ \int_{x_{k-1}}^{x_k} (\phi_t + f_x)\psi dx \right\} = 0. \tag{13}$$

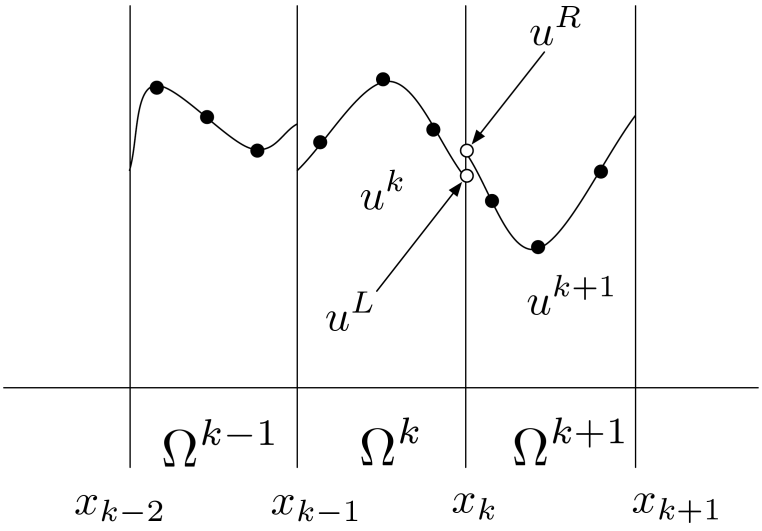

Fig. 1. Subdivision of the physical domain into K elements, u represents the unknown.

To use the Legendre polynomial approximation on each element, every interval (x_{k-1}, x_k) is mapped onto the reference interval $\xi \in [-1, 1]$, by the affine mapping

$$x = x_{k-1} + \frac{\xi + 1}{2}\Delta x_k, \tag{14}$$

where $\Delta x_k = x_k - x_{k-1}$. Then

$$dx = \frac{\Delta x_k}{2} d\xi, \qquad \frac{\partial}{\partial x} = \frac{2}{\Delta x_k}\frac{\partial}{\partial \xi}, \tag{15}$$

so that on the reference interval, the weak form of the PDE becomes

$$\sum_{k=1}^{K}\left\{\frac{\Delta x_k}{2}\int_{-1}^{1}\phi_t\psi d\xi+\int_{-1}^{1}f_\xi\psi d\xi\right\}=0. \tag{16}$$

Now the solution and the fluxes in each element are approximated by the Legendre orthogonal interpolating polynomial, which is written in the Lagrange form

$$\begin{aligned}\phi(\xi,t)\approx\phi^N(\xi,t)&=\sum_{i=0}^{N}\phi^N(\xi_i,t)\ell_i(\xi),\\ f(\xi,t)\approx f^N(\xi,t)&=\sum_{i=0}^{N}f^N(\xi_i,t)\ell_i(\xi),\end{aligned} \tag{17}$$

where ξ_i are the LG nodes. The notation $\phi_i^N(t)\equiv\phi^N(\xi_i,t)$ is used in the following to simplify the notation. The nodal (grid point) values of the fluxes are computed from the grid point values of the solution, i.e., $f_\xi^N=f\left(\phi_\xi^N\right)$. Note that ϕ_ξ^N is not the nodal value of $\phi(\xi)$, but the result of solving the unknowns in the problem. Therefore

$$\phi^N(\xi)=\sum_{i=0}^{N}\phi_i^N\ell_i(\xi),\qquad\text{and}\qquad I_N\phi(\xi)=\sum_{i=0}^{N}\phi_i\ell_i(\xi), \tag{18}$$

are different. The former is the solution of the discretized PDE, while the latter is the spectral interpolation of the exact solution of the PDE. The same applies to the fluxes. It should also be noticed that a different polynomial order N, and size of the element Δx_k, are permitted for each subdivision.

The approximate solution (17) is substituted into the weak form in the reference element (16) to obtain

$$\frac{\Delta x_k}{2}\int_{-1}^{1}\phi_t^N\psi d\xi+\int_{-1}^{1}f_\xi^N\psi d\xi=0. \tag{19}$$

As the method is of a Galerkin type, the test function ψ can be also written as

$$\psi=\sum_{i=0}^{N}\psi_i\ell_i(\xi), \tag{20}$$

that can be substituted into (19) to obtain

$$\sum_{j=0}^{N}\left\{\frac{\Delta x_k}{2}\int_{-1}^{1}\phi_t^N\ell_j(\xi)d\xi+\int_{-1}^{1}f_\xi^N\ell_j(\xi)d\xi\right\}\psi_j=0. \tag{21}$$

To guarantee that (16) holds for any smooth enough function is equivalent to guarantying that the coefficients of the Lagrange polynomial that represent the test functions ψ_j in (21) are independent from each other, hence

$$\frac{\Delta x_k}{2}\int_{-1}^{1}\phi_t^N\ell_j(\xi)d\xi+\int_{-1}^{1}f_\xi^N\ell_j(\xi)d\xi=0,\qquad j=0,1,\ldots,N. \tag{22}$$

Let us recall that (22) is forcing the residual to be zero in an integral way. Or more accurately, compels the residual to be orthogonal to the approximation space locally within each element.

Now (22) is integrated by parts to separate the interior from the interface contributions

$$\frac{\Delta x_k}{2}\int_{-1}^{1}\phi_t^N\ell_j(\xi)d\xi + f^N\ell_j\Big|_{-1}^{1} - \int_{-1}^{1}f^N\ell_j'(\xi)d\xi = 0, \qquad j = 0,1,\ldots,N. \tag{23}$$

The representation (17) is inserted into the weak form (23) to become

$$\frac{\Delta x_k}{2}\sum_{i=0}^{N}\dot{\phi}_i^N\int_{-1}^{1}\ell_i(\xi)\ell_j(\xi)d\xi + f^N\ell_j\Big|_{-1}^{1} - \sum_{i=0}^{N}f_i^N\int_{-1}^{1}\ell_i(\xi)\ell_j'(\xi)d\xi = 0, \qquad j = 0,1,\ldots,N, \tag{24}$$

where $\dot{\phi}_i^N \equiv \dfrac{d\phi_i^N}{dt}$. To be consistent with the nodal Galerkin methodology, integral inner products are approximated via quadrature formulas rather than solved analytically. As explained before, the LG nodes are used for their higher accuracy. The approximation of both integrals is exact with this set of nodes such that

$$\int_{-1}^{1}\ell_i(\xi)\ell_j(\xi)d\xi = \sum_{k=0}^{N}\ell_i(\xi_k)\ell_j(\xi_k)w_k = w_j\delta_{i,j} \tag{25}$$

and

$$\int_{-1}^{1}\ell_i(\xi)\ell_j'(\xi)d\xi = \sum_{k=0}^{N}\ell_i(\xi_k)\ell_j'(\xi_k)w_k = \ell_j'(\xi_i)w_i. \tag{26}$$

Substituting (25) and (26) into (24) and simplifying the sums we obtain

$$\frac{\Delta x_k}{2}\dot{\phi}_j^N w_j + f^N\ell_j\Big|_{-1}^{1} - \sum_{i=0}^{N}f_i^N\ell_j'(\xi_i)w_i = 0, \qquad j = 0,1,\ldots,N. \tag{27}$$

Recall that the flux function f^N is the combination of the advective and viscous fluxes $f^N = f_A^N - f_V^N$. The advective flux f_A^N can be directly evaluated at the computation nodes. On the contrary, the viscous flux f_V^N involves a derivative of the solution, and should be treated consistently with the rest of the scheme. Let us write an auxiliary viscous equation,

$$f_V - \Gamma\phi_x = 0, \qquad x \in (0,L). \tag{28}$$

Equation (28) is solved with the same procedure as applied to Eqs. (11)–(27) obtaining,

$$\frac{\Delta x_k}{2}f_{Vj}^N w_j - \Gamma\phi^N\ell_j\Big|_{-1}^{1} + \sum_{i=0}^{N}\Gamma\phi_i^N\ell_j'(\xi_i)w_i = 0, \qquad j = 0,1,\ldots,N. \tag{29}$$

This approach is known as Bassi-Rebay 1 (BR1) approach [4]. For alternatives to the BR1 approach, see [2].

In the final step, the elements are coupled and the fluxes at the element boundaries are replaced by the numerical flux

$$\frac{\Delta x_k}{2}\dot{\phi}_j^N w_j + f^{N*}\ell_j\Big|_{-1}^{1} - \sum_{i=0}^{N}f_i^N\ell_j'(\xi_i)w_i = 0, \qquad j = 0,1,\ldots,N, \tag{30}$$

and similarly for the auxiliar viscous equation,

$$\frac{\Delta x_k}{2}f_{Vj}^N w_j - \Gamma\phi^{N*}\ell_j\Big|_{-1}^{1} + \sum_{i=0}^{N}\Gamma\phi_i^N\ell_j'(\xi_i)w_i = 0, \qquad j = 0,1,\ldots,N. \tag{31}$$

These numerical fluxes $f^{N*} = f_A^{N*} - f_V^{N*}$ and ϕ^{N*} are a function of the element and its immediate neighbor (or a physical boundary). For the advective flux f_A^{N*} a Riemann problem should be solved [34]. The Riemann solver calculates a value for the fluxes, taking into account the values at each side of the discontinuity (u^L and u^R in Fig. 1) and the directions of transfer of information in the equation. The viscous contributions (f_V^{N*} and ϕ^{N*}) are computed taking the mean value of the element and its immediate neighbor (or physical boundary).

It should be noticed that if the source term S in the conservation law (Eq. (11)) is different from zero, Eq. (30) becomes

$$\frac{\Delta x_k}{2}\dot{\phi}_j^N w_j + f^{N*}\ell_j\big|_{-1}^{1} - \sum_{i=0}^{N} f_i^N \ell_j'(\xi_i) w_i = \frac{\Delta x_k}{2} S_j^N w_j, \qquad j = 0, 1, \ldots, N, \tag{32}$$

where S_j^N is the source term function evaluated at the grid nodes.

The resulting system of ODE (32) is the discretization of problem (11) and can be solved, as in the Chebyshev collocation method, by any explicit or implicit time stepping method, e.g., Runge-Kutta.

3. Results

The nonlinear steady Burgers' equation used for comparison is

$$\upsilon\frac{d\upsilon}{dx} = \mu\frac{d^2\upsilon}{dx^2} + S(x) \;\Rightarrow\; \frac{d}{dx}\left(\frac{1}{2}\upsilon^2 - \mu\frac{d\upsilon}{dx}\right) = S(x). \tag{33}$$

In terms of the description of both methods in the previous section the generic unknown is $\upsilon = \phi$, the convective flux is $\rho\upsilon = 1/2\upsilon$ and the diffusion coefficient is $\Gamma = \mu$.

Several tests with this equation have been carried out. As it was the first comparison of these two methods the interest was mainly focused on their ability to handle nontrivial sources in convection-dominated flows. In the first test, the nonlinear advection equation contains a source that causes an internal layer to appear in the region close to the left boundary. The second test introduces the diffusion term but with no source. The solution in this case is a hyperbolic tangent that develops a boundary layer close to the right end of the domain whose thickness is of the order of μ. The third test introduces a source that provides a manufactured solution with a sinusoidal shape. This source can be tuned to obtain different solutions with various wavelengths.

Let us notice that for the DGSEM the test cases discussed here are always solved in a domain of length $L = 2$. This means that the relationship between the number of elements/finite volumes K, and the size of each element Δx is

$$\Delta x = \frac{2}{K}. \tag{34}$$

In the DGSEM the coefficient matrix is $K * (N + 1) \times K * (N + 1)$, N being the order of the polynomial that approximates the solution in every interval. With ENATE the solution for υ is only obtained at the nodes as every single coefficient in the integral expressions can be obtained as function of these. The coefficient matrix is $(K-1)\times(K-1)$ as two nodes are located at the domain boundaries. To compare both graphically Δx has been chosen as the variable in the horizontal axis. For all cases three Hermite polynomials were employed in ENATE: cubic, quintic and septic, and two polynomials for each element in the DGSEM: a fourth degree and a ninth degree polynomial. All results are presented in terms of the energy norm of the error vector $\|\upsilon - \upsilon^N\|_{L_2}$.

3.1. Test case 1

The exact solution of the nonlinear convection equation with source is

$$\frac{1}{2}v^2(x) = \frac{1}{2}v^2(x_{lb}) + \int_{x_{lb}}^{x} S(x')\,dx', \tag{35}$$

where x_{lb} is the left boundary of the domain and x' is a dummy variable. The source term is defined $S(x) = 20\tanh(20(0.75+x))/\cosh^2(20(0.75+x))$, such that the exact solution is $v(x) = \tanh(20(0.75+x))$. The results obtained by the DGSEM are given in Fig. 2. The results obtained by ENATE are exact. As explained in [27] ENATE can give the exact solution if the source has an analytical primitive. We intentionally present these results to show that if the source produces an internal layer the DGSEM requires element sizes to be very small. It is relatively difficult for the DGSEM to reproduce a steep internal layer inside an element even with a high-degree polynomial.

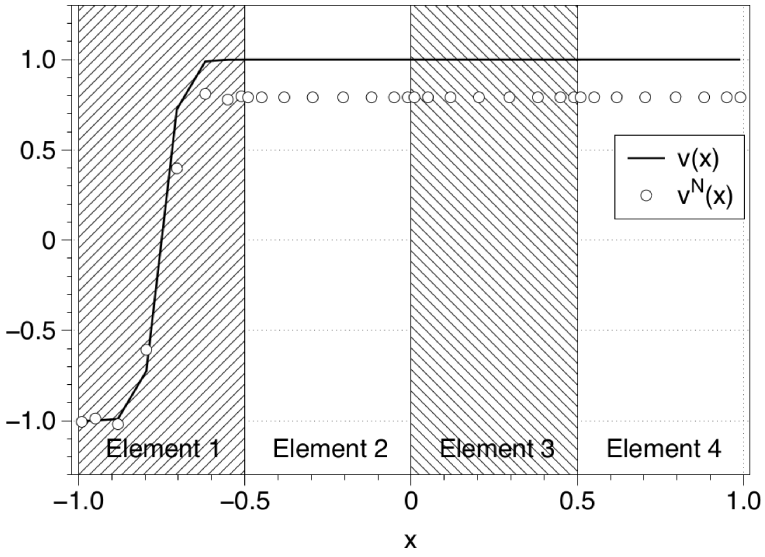

Fig. 2. The DGSEM results. First test case, $v(x)$ is the exact solution and v^N the approximated one.

3.2. Test case 2

In the second test case the source is set to zero. Two cases have been run for values of the viscosity $\mu = 0.1$ and $\mu = 5 \times x10^{-3}$. The exact solution is given by

$$v(x) = C_1 \tanh\left[\frac{C_1}{2\mu}(1-x)\right]. \tag{36}$$

C_1 has been adopted such that the value of the solution at $x = 0$ is 1. The boundary conditions employed are $v(-1) = v_{ex}(-1)$ and $v(1) = 0$. This case was run with cubic, quintic and septic Hermite polynomials for ENATE, and two polynomials for each element in the DGSEM: a fourth degree and a ninth degree polynomial.

The norms for $\mu = 0.1$ are given in Fig. 3. This viscosity value produces a relatively smooth solution over the whole domain. As can be appreciated the results are very consistent with the polynomial degree, independently of the method adopted. Cubic Hermite, for instance, has a lower order of convergence and less accuracy than the DGSEM with a fourth order polynomial. The

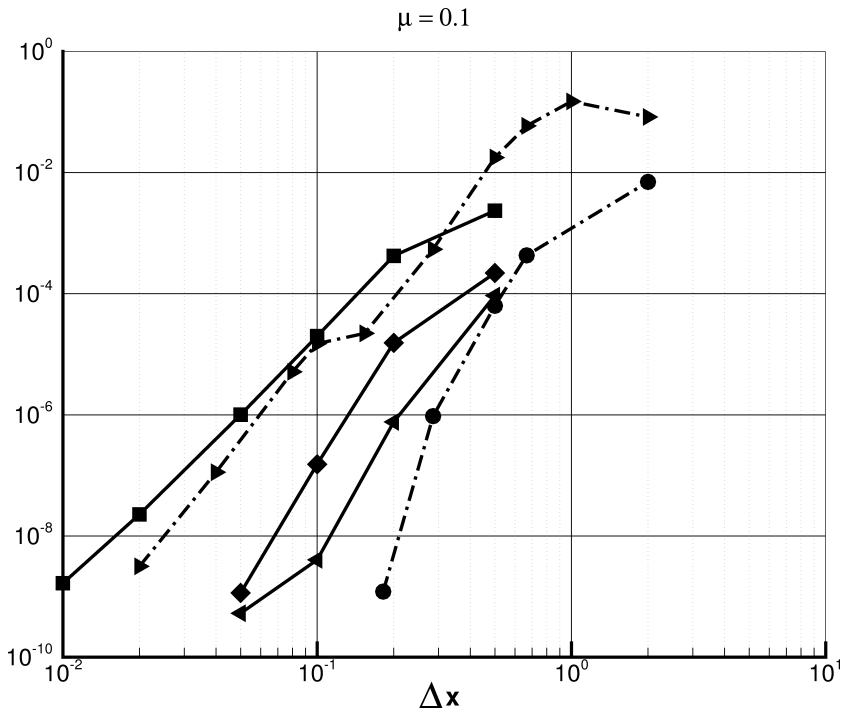

Fig. 3. Test 2: Energy norm for the error $||v - v^N||_{L_2}$ against element size Δx for $\mu = 0.1$. Solid lines represent ENATE results: cubic (square), quintic (diamond) and septic (left triangle). Dashed lines are the DGSEM: fourth degree polynomial (right triangle) and fourth degree polynomial (circle).

obtained order of convergence for ENATE polynomials is that predicted theoretically [27]: fourth order for cubic, sixth order for quintic and eighth order for septic. The accuracy of the schemes with the highest degree is exceptional: the DGSEM has a L_2 norm of 10^{-6} with six elements and

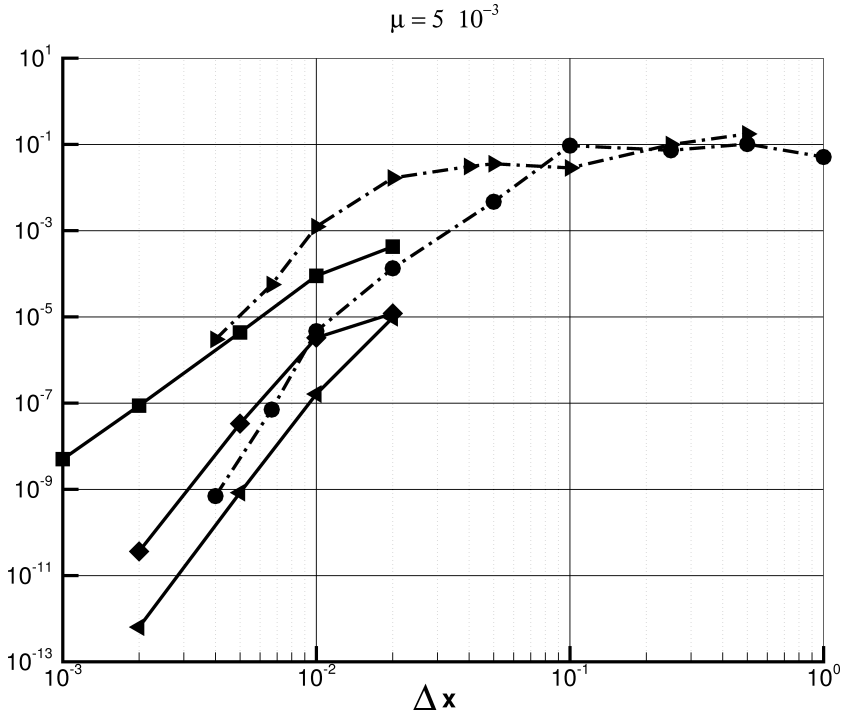

Fig. 4. Test 2: Energy norm for the error $||v - v^N||_{L_2}$ against element size Δx for $\mu = 0.005$. Solid lines represent ENATE results: cubic (square), quintic (diamond) and septic (left triangle). Dashed lines are the DGSEM: fourth degree polynomial (right triangle) and fourth degree polynomial (circle).

ENATE has a slightly lower one with ten intervals. The norms for $\mu = 0.005$ are provided in Fig. 4. The DGSEM produces very low norms with few nodes where ENATE cannot obtain a converged solution. When both reach a converged solution the behavior is similar with the order of convergence for the DGSEM starting to show the predicted asymptotic value. As in the first case, there is a boundary layer near $x = 1$ that the DGSEM is not able to reproduce well, which makes ENATE better behaved for this particular case, that is, its asymptotic order of convergence is reached for higher Δx.

3.3. Test case 3

In this test case the source is chosen so the solution is

$$\upsilon(x) = 2 - A\sin(\sigma\pi x). \tag{37}$$

We present two solutions for values of parameter $\sigma = 1$ and 5. $\sigma = 1$ represents a sinusoidal solution that spans one wavelength over the whole domain and $\sigma = 5$ represents a solution with a wavelength one fifth of the previous one. The boundary values are set to the exact ones. The source is slightly complicated due to the nonlinear nature of the original equation and is not detailed here.

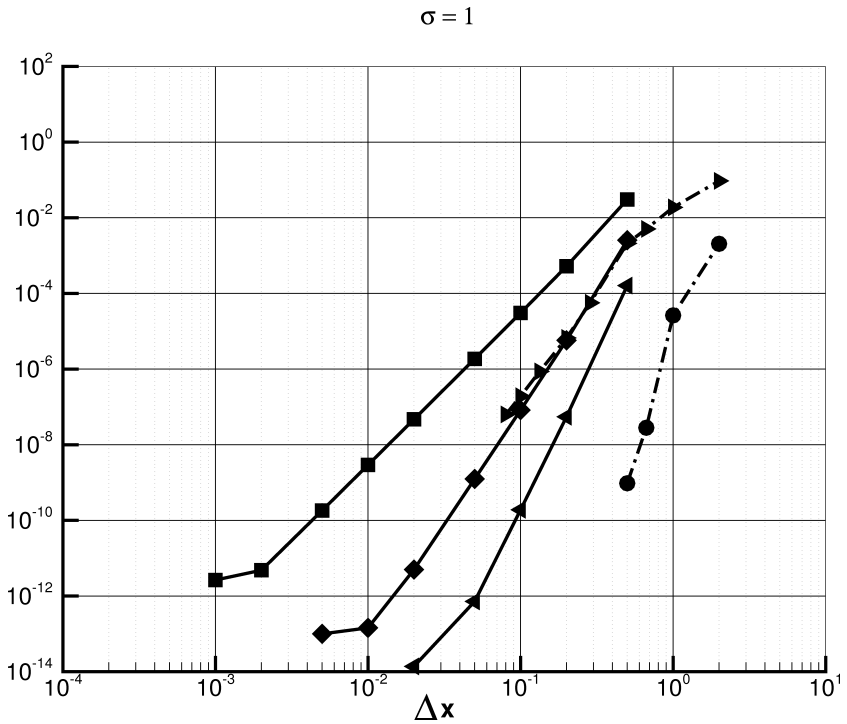

Fig. 5. Test 3: Energy norm for the error $\|\upsilon - \upsilon^N\|_{L_2}$ against element size Δx for $\sigma = 1$. Solid lines represent ENATE results: cubic (square), quintic (diamond) and septic (left triangle). Dashed lines are the DGSEM: fourth degree polynomial (right triangle) and fourth degree polynomial (circle).

The results are again consistent. Both approaches reach the asymptotic range with as few as 10 nodes. The only slight discrepancy with the theoretical expected orders is, that a fourth order DGSEM follows the same order of convergence as quintic Hermite, showing that the DGSEM has a better performance than ENATE in this case. Both approaches seem to deal with the source terms in an accurate manner.

The results for a solution with a shorter wavelength are similar. The order of convergence is consistent with the polynomial degree with the DGSEM showing superior performance, the behavior of the highest degree polynomial for both approaches being extremely good. The DGSEM has a L_2 norm of 10^{-8} with fifteen elements and ENATE provides the same norm with forty.

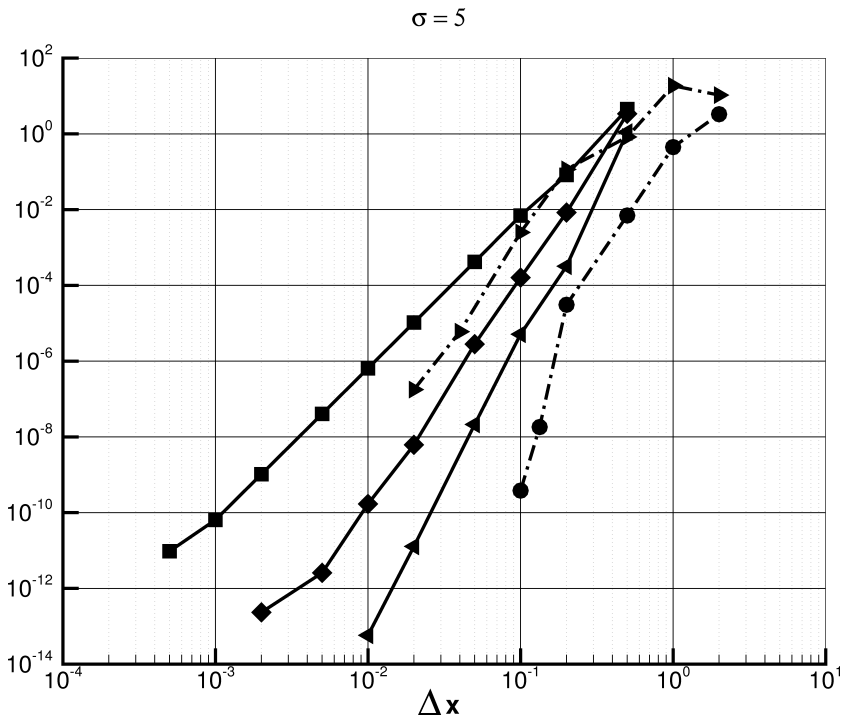

Fig. 6. Test 3: Energy norm for the error $\|v - v^N\|_{L_2}$ against element size Δx for $\sigma = 5$. Solid lines represent ENATE results: cubic (square), quintic (diamond) and septic (left triangle). Dashed lines are the DGSEM: fourth degree polynomial (right triangle) and fourth degree polynomial (circle).

4. Conclusions

A comparison of the performance of two high-order approaches in the calculation of the 1D nonlinear Burgers' equation has been performed. The results of both approaches are very good and in some cases excellent. In general terms, the DGSEM performs better than ENATE, with the error norms behaving in accordance with the polynomial degree chosen. However, there are still some drawbacks. The DGSEM is not able to reproduce adequately a steep layer inside an element even with high degree polynomials and is outperformed by ENATE in that case. ENATE is not able to calculate a converged solution with large Δx where the DGSEM finds one.

ENATE is a method that has been recently proposed, and as such it requires a careful assessment in various instances. It seemed to us that as the DGSEM is a well established high-order approach that has long shown its good performance, a thorough comparison of these two methods in a bunch of 1D cases was of interest, especially in terms of accuracy. As a matter of fact, the comparison of these two approaches in 1D cases is very limited and a study with their comparisons in 2D is also in preparation. The DGSEM does not need any additional treatment but ENATE, as indicated in [27], requires extra pseudo-source terms, coming from the derivatives in the other coordinate direction, to be approximated accurately.

Acknowledgements

Dr. Arici was supported by the Scientific and Technological Research of Turkey (TÜBİTAK) under 2219-Grant Program.

Dr. Pascau has been (partially) funded by Gobierno de Aragón whose motto is 'Building Europe from Aragón' and by FEDER funding from the European Union (Grupo Consolidado de Mecánica de Fluidos Computacional T21).

References

[1] C. Acosta, D.A. Kopriva. Discontinuous Galerkin spectral element approximations on moving meshes. *Journal of Computational Physics*, **230**(5): 1876–1902, 2011.

[2] D.N. Arnold, F. Brezzi, B. Cockburn, L.D. Marini. Unified analysis of discontinuous Galerkin methods for elliptic problems. *SIAM Journal on Numerical Analysis*, **39**(5): 1749–1779, 2001.

[3] F. Bassi, A. Crivellini, D.A. Di Pietro, S. Rebay. An artificial compressibility flux for the discontinuous Galerkin solution of the incompressible Navier-Stokes equations. *Journal of Computational Physics*, **218**(2): 794–815, 2006.

[4] F. Bassi, S. Rebay. A high-order accurate discontinuous finite element method for the numerical solution of the compressible Navier-Stokes equations. *Journal of Computational Physics*, **131**(2): 267–279, 1997.

[5] C.E. Baumann. *An hp-Adaptive Discontinuous Finite Element Method for Computational Fluid Dynamics*. PhD thesis, University of Texas at Austin, 1997.

[6] K. Black. A conservative spectral element method for the approximation of compressible fluid flow. *Kybernetika*, **35**(1): 133–146, 1999.

[7] K. Black. Spectral element approximation of convection-diffusion type problems. *Applied Numerical Mathematics*, **33**(1–4): 373–379, 2000.

[8] C. Canuto, M.Y. Hussaini, A. Quarteroni, T.A. Zang. *Spectral Methods*. Fundamentals in Single Domains. Springer, Berlin, 2006.

[9] N. Castel, G. Cohen, M. Duruflé. Application of discontinuous Galerkin spectral method on hexahedral elements for aeroacoustic. *Journal of Computational Acoustics*, **17**(2): 175–196, 2009.

[10] S. Deng. Numerical simulation of optical coupling and light propagation in coupled optical resonators with size disorder. *Applied Numerical Mathematics*, **57**(5–7): 475–485, 2007.

[11] S. Deng, W. Cai, V. Astratov. Numerical study of light propagation via whispering gallery modes in microcylinder coupled resonator optical waveguides. *Optics Express*, **12**(26): 6468–6480, 2004.

[12] S. Fagherazzi, D.J. Furbish, P. Rasetarinera, M.Y. Hussaini. Application of the discontinuous spectral Galerkin method to groundwater flow. *Advances in Water Resources*, **27**(2): 129–140, 2004.

[13] S. Fagherazzi, P. Rasetarinera, M.Y. Hussaini. Numerical solution of the dambreak problem with a discontinuous Galerkin method. *Journal of Hydraulic Engineering*, **130**(6): 532–539, 2004.

[14] E. Ferrer. *A High Order Discontinuous Galerkin-Fourier Incompressible 3D Navier-Stokes Solver with Rotating Sliding Meshes for Simulating Cross-Flow Turbines*. PhD thesis, University of Oxford, 2012.

[15] E. Ferrer, R.H.J. Willden. A high order discontinuous Galerkin finite element solver for the incompressible Navier-Stokes equations. *Computers & Fluids*, **46**(1): 224–230, 2011.

[16] E. Ferrer, R.H.J. Willden. A high order discontinuous Galerkin-Fourier incompressible 3D Navier-Stokes solver with rotating sliding meshes. *Journal of Computational Physics*, **231**(21): 7037–7056, 2012.

[17] F.X. Giraldo, J.S. Hesthaven, T. Warburton. Nodal high-order discontinuous Galerkin methods for the spherical shallow water equations. *Journal of Computational Physics*, **181**(2): 499–525, 2002.

[18] F.X. Giraldo, M. Restelli. A study of spectral element and discontinuous Galerkin methods for the Navier-Stokes equations in nonhydrostatic mesoscale atmospheric modeling: Equation sets and test cases. *Journal of Computational Physics*, **227**(8): 3849–3877, 2008.

[19] G.E. Karniadakis, S. Sherwin. *Spectral/hp Element Methods for Computational Fluid Dynamics*. Oxford Science Publications, 2005.

[20] M. Kompenhans, G. Rubio, E. Ferrer, E. Valero. Adaptation strategies for high order discontinuous Galerkin methods based on Tau-estimation. *Journal of Computational Physics*, **306**: 216–236, 2016.

[21] M. Kompenhans, G. Rubio, E. Ferrer, E. Valero. Comparisons of p-adaptation strategies based on truncation-and discretisation-errors for high order discontinuous Galerkin methods. *Computers & Fluids*, **139**: 36–46, 2016.

[22] D.A. Kopriva. Metric identities and the discontinuous spectral element method on curvilinear meshes. *Journal of Scientific Computing*, **26**(3): 301–327, 2006.

[23] D.A. Kopriva. *Implementing Spectral Methods for Partial Differential Equations: Algorithms for Scientists and Engineers*. Springer Science & Business Media, 2009.

[24] D.A. Kopriva, S.L. Woodruff, M.Y. Hussaini. Computation of electromagnetic scattering with a non-conforming discontinuous spectral element method. *International Journal for Numerical Methods in Engineering*, **53**(1): 105–122, 2002.

[25] S. Mao, C.A. Luongo, D.A. Kopriva. Discontinuous Galerkin spectral element simulation of quench propagation in superconducting magnets. *IEEE Transactions on Applied Superconductivity*, **15**(2): 1675–1678, 2005.

[26] A. Pascau. An exact discretization for a transport equation with piecewise-constant coefficients and arbitrary source. *Computers and Fluids*, **75**: 42–50, 2013.

[27] A. Pascau, M. Arici. An accurate discretization for an inhomogeneous transport equation with arbitrary coefficients and source. *Computers and Fluids*, **125**: 101–115, 2016.

[28] P. Rasetarinera, M.Y. Hussaini. An efficient implicit discontinuous spectral Galerkin method. *Journal of Computational Physics*, **172**(2): 718–738, 2001.

[29] P. Rasetarinera, D.A. Kopriva, M.Y. Hussaini. Discontinuous spectral element solution of acoustic radiation from thin airfoils. *AIAA Journal*, **39**(11): 2070–2075, 2001.

[30] W.H. Reed, T.R. Hill. *Triangular Mesh Methods for the Neutron Transport Equation*. Los Alamos Report LA-UR-73-479, 1973.

[31] M. Restelli, F.X. Giraldo. A conservative discontinuous Galerkin semi-implicit formulation for the Navier-Stokes equations in nonhydrostatic mesoscale modeling. *SIAM Journal on Scientific Computing*, **31**(3):2231–2257, 2009.

[32] D. Stanescu, M. Hussaini, F. Farassat. Aircraft engine noise scattering – A discontinuous spectral element approach. [In:] *40th AIAA Aerospace Sciences Meeting & Exhibit*, Reston, Virigina, American Institute of Aeronautics and Astronautics, 2012.

[33] D. Stanescu, J. Xu, M.Y. Hussaini, F. Farassat. Computation of engine noise propagation and scattering off an aircraft. *International Journal of Aeroacoustics*, **1**(4): 403–420, 2009.

[34] E.F. Toro. *Riemann Solvers and Numerical Methods for Fluid Dynamics. A Practical Introduction*. Springer, 2009.